Numerical study on the discharge characteristics and nonlinear behaviors of atmospheric pressure coaxial electrode dielectric barrier discharges*

Ding-Zong Zhang(张定宗)[1,†], Yan-Hui Wang(王艳辉)[2,‡], and De-Zhen Wang(王德真)[2]

[1] School of Physics and Electronic Engineering, Hengyang Normal University, Hengyang 421008, China
[2] School of Physics and Optoelectronic Technology, Dalian University of Technology, Dalian 116024, China

(Received 29 December 2016; revised manuscript received 22 March 2017; published online 20 April 2016)

The discharge characteristics and temporal nonlinear behaviors of the atmospheric pressure coaxial electrode dielectric barrier discharges are studied by using a one-dimensional fluid model. It is shown that the discharge is always asymmetrical between the positive pulses and negative pulses. The gas gap severely affects this asymmetry. But it is hard to acquire a symmetrical discharge by changing the gas gap. This asymmetry is proportional to the asymmetric extent of electrode structure, namely the ratio of the outer electrode radius to the inner electrode radius. When this ratio is close to unity, a symmetrical discharge can be obtained. With the increase of frequency, the discharge can exhibit a series of nonlinear behaviors such as period-doubling bifurcation, secondary bifurcation and chaotic phenomena. In the period-doubling bifurcation sequence the period-n discharge becomes more and more unstable with the increase of n. The period-doubling bifurcation can also be obtained by altering the discharge gas gap. The mechanisms of two bifurcations are further studied. It is found that the residual quasineutral plasma from the previous discharges and corresponding electric field distribution can weaken the subsequent discharge, and leads to the occurrence of bifurcation.

Keywords: atmospheric dielectric-barrier discharge, numerical simulation, nonlinear behaviors

PACS: 52.65.–y, 05.45.Pq, 52.80.–s **DOI:** 10.1088/1674-1056/26/6/065206

1. Introduction

Owing to the ability to generate non-equilibrium plasma and high-density active species and to dispense with a vacuum chamber, the atmospheric pressure dielectric barrier discharges (DBDs) currently acquire wide applications in surface modification, pollution control, thin-film deposition and biological sterilization.[1–4] The DBDs can be realized when at least one of its electrodes is covered by a dielectric layer. Usually, there are three kinds of electrode structures: parallel plate structure, coaxial electrode structure and needle-plate structure. In the space domain of the atmospheric pressure DBDs, the discharge can exhibit different spatial structures including filamentary discharge, diffuse discharge and self-organized patterned discharge.[5,6] In past decades, the discharge characteristics and formation mechanisms of these three structures have been extensively studied. In addition to these spatial behaviors, atmospheric pressure DBDs should also in nature have abundant temporal nonlinear behaviors such as period-doubling bifurcation, quasiperiodic behaviors and chaotic phenomena. Recently, these nonlinear behaviors have been widely observed by numerical simulation and experiment.[7–11] Significant advances have been made both in their fundamental mechanism and in their dependence on the discharge parameters. But most of these papers focused on the parallel plate structure and needle-plate structure. There is a distinct lack of papers covering the nonlinear behaviors in coaxial electrode structure. The temporal nonlinear behavior mechanisms in coaxial electrode DBDs and the corresponding effects of discharge parameters on these nonlinear behaviors are far from being understood. A typical characteristic of the discharge in the coaxial electrodes is that the discharge current peaks between the positive pulses and negative pulses are never equal to each other, namely the discharge is asymmetrical. It is still not clear whether the gas gap and electrode structure have significant effects on this asymmetry. To throw light on these issues, in this paper we present a one-dimensional fluid model to investigate the temporal nonlinear behaviors and discharge characteristics of the atmospheric pressure coaxial electrode DBDs.

2. Model

Figure 1 shows the atmospheric pressure DBD setup in this paper. The inner electrode with an outer radius R_0 is driven by a sinusoidal voltage. The outer electrode with an inner radius R_2 is jacked on the outside of a quartz glass tube

*Project supported by the National Natural Science Foundation of China (Grant Nos. 11447244 and 11405208), the Science Foundation of Hengyang Normal University, China (Grant No. 14B41), and the Hunan Provincial Applied Basic Research Base of Optoelectronic Information Technology, China (Grant No. GDXX010).

†Corresponding author. E-mail: Zhangdingzong2006@163.com
‡Corresponding author. E-mail: wangyh@dlut.edu.cn

© 2017 Chinese Physical Society and IOP Publishing Ltd

and is grounded. The R_1 represents the inner radius of the quartz glass tube. The axial length of the electrodes is L and the working gas is pure helium.

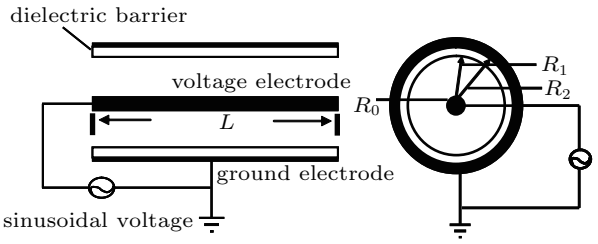


Fig. 1. DBD setup in this paper.

Like our previous work,[11] the fundamental model is chosen. In the one-dimensional limit, the continuity equation and momentum equation can be given as follows:

$$\frac{\partial n_{\mathrm{e,i}}(r,t)}{\partial t}+\frac{1}{r}\frac{\partial[r j_{\mathrm{e,i}}(r,t)]}{\partial r}=S_{\mathrm{e,i}}(r,t), \tag{1}$$

$$j_{\mathrm{e,i}}(r,t)=-D_{\mathrm{e,i}}\frac{\partial}{\partial r}[n_{\mathrm{e,i}}(r,t)]\mp\mu_{\mathrm{e,i}}n_{\mathrm{e,i}}E(r,t), \tag{2}$$

where n and j are the density and flux, D and μ represent the diffusion and mobility coefficient, the subscripts e and i represent the electron and ion, and the minus and plus signs in Eq. (2) refer to electrons and ions, respectively; S is the source term, in which only the direct ionization and electron–He^+ recombination are considered. Thus S_{e} and S_{i} have the same form as follows:

$$S_{\mathrm{e}}=S_{\mathrm{i}}=\alpha\mu_{\mathrm{e}}|E(r,t)|n_{\mathrm{e}}(r,t)-\beta n_{\mathrm{i}}(r,t)n_{\mathrm{e}}(r,t), \tag{3}$$

where α is the Townsend ionization coefficient, β is the recombination coefficient, and their values are obtained from Refs. [12] and [13]. E is the electric field, which is calculated from the Poisson equation

$$\frac{1}{r}\frac{\partial[rE(r,t)]}{\partial r}=\frac{e}{\varepsilon\varepsilon_0}[-n_{\mathrm{e}}(r,t)+n_{\mathrm{i}}(r,t)], \tag{4}$$

where ε_0 is the vacuum permittivity. The value of ε is a function of r. In the gas gap, $\varepsilon=1$, while in the dielectric layer, ε equals the relative permittivity ε_{B}. In this paper, the current conservation equation is used for calculating the electric field. This technique is widely used to simulate the atmospheric pressure DBDs.[14–18]

$$\varepsilon_0\varepsilon\frac{\partial E(r,t)}{\partial t}+j_{\mathrm{c}}(r,t)=j_0(r,t), \tag{5}$$

where $\varepsilon_0\varepsilon\partial E/\partial t$, j_{c}, and j_0 are, respectively, the displacement, conduction, and discharge current density. The total discharge current $i_{\mathrm{T}}(t)$ can be obtained through multiplying Eq. (5) by $2\pi rL$ and then integrating it between two electrodes as follows:

$$i_{\mathrm{T}}(t)=\frac{2\pi L\varepsilon_0\varepsilon_{\mathrm{B}}}{\varepsilon_{\mathrm{B}}\ln(R_1/R_0)+\ln(R_2/R_1)}\times\left[\frac{\partial V(t)}{\partial t}+\frac{1}{\varepsilon_0}\int_{R_0}^{R_1}j_{\mathrm{c}}(r,t)\,\mathrm{d}r\right], \tag{6}$$

where $V(t)$ is the voltage applied to the two coaxial electrodes. The corresponding discharge current densities at different radii are calculated from the relation $j_0(r,t)=i_{\mathrm{T}}(t)/2\pi rL$. The surface charge density q accumulated on the dielectric barrier is given by

$$q(t)=\int_0^t j_{\mathrm{c}}(R_1,t')\,\mathrm{d}t'. \tag{7}$$

The above equations (1)–(7) are solved using the Schartetter–Gummel scheme.[19] The initial density of electron and ion are assumed to be spatially uniform and both are 10^7 cm^{-3}.

3. Results and discussion

Unless otherwise specified, the following parameters are used hereafter. The outer radius of the inner electrode R_0, inner radius of the dielectric layer R_1, and inner radius of the outer electrode R_2 are 0.2 cm, 0.8 cm, and 0.9 cm, respectively. The discharge gas gap d is 0.6 cm, the corresponding pressure is 760 Torr (1 Torr = 1.33322×10^2 Pa), and the gas temperature is 300 K. The relative permittivity ε_{B} is 7.5 and the dielectric layer thickness d_{B} is 0.1 cm. The amplitude of the voltage is 2.4 kV and the axial length of the electrodes L is 10 cm. The secondary electron emission coefficient caused by the ion bombarding instantaneous cathode is set to be 0.01.[20]

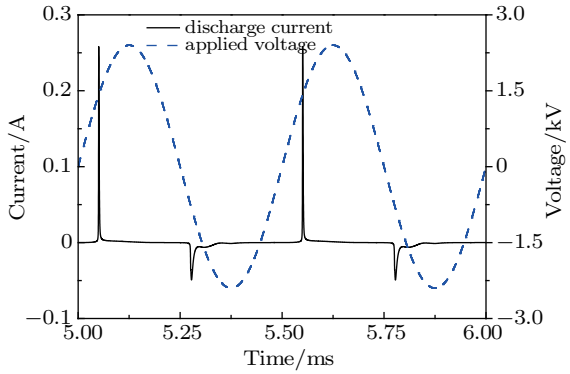


Fig. 2. (color online) Curves of voltage–current waveform versus time at 2 kHz.

Figure 2 shows the curve of voltage–current waveforms evolving with time at 2 kHz. It is clear that the discharge is an asymmetric single pulse discharge, which consists well with the experimental and numerical results.[21,22] The current peak at positive half cycle is 0.258 A, while the peak for the negative half cycle is only 0.0492 A. This is very different from the scenario of the typical discharge in the parallel-plate electrode, in which the positive current peak equals the negative current peak, namely the discharge is symmetrical. Recent studies show that the symmetrical discharge in the parallel-plate electrode can become asymmetrical with the increase of the gas

gap.[11,23–25] Conversely, the discharge can become symmetrical by reducing the gas gap.

To determine whether the asymmetry of the coaxial electrode DBD is also related to the gas gap, we study the effect of the gas gap on the discharge. In these calculations, the gas gap is changed by altering R_1. To simplify the descriptions, we use A_1/A_2 to represent the degree of current asymmetry. Here, A_1 is the positive current peak and A_2 is the negative current peak. Figure 3 shows the evolutions of A_1/A_2 at different gas gaps. It is found that the A_1/A_2 decreases exponentially with the decrease of gas gap. But when the gas gap decreases to 0.59 cm, the further decreasing of the gas gap results in the increase of A_1/A_2, accompanied by the emergence of multi pulse discharge mode. Figure 4 shows the voltage–current waveforms of this multi pulse discharge, where the gas gap is 0.58 cm. In this figure both the peak and number of the discharge pulses are asymmetrical. The positive current peak is about 5.33 times the negative current peak, and there are two current pulses in a negative half-cycle of the driven voltage, while only one current pulse is in a positive half-cycle. These suggest that the gas gap has an important effect on the asymmetry of the atmospheric-pressure coaxial electrode DBD. The degree of current asymmetry can be reduced exponentially by reducing the gas gap. But it may not obtain a symmetrical single pulse discharge in this way, because at small gas gap the multi-pulse discharge appears.

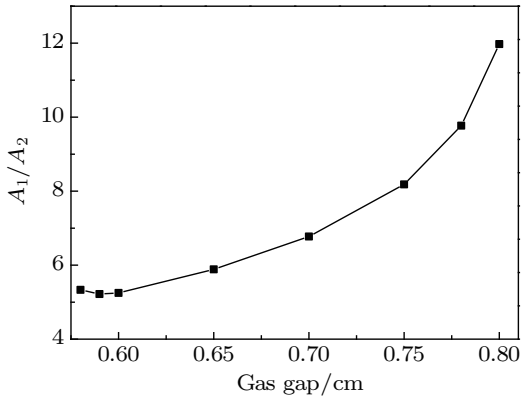


Fig. 3. Variation of A_1/A_2 with gas gap.

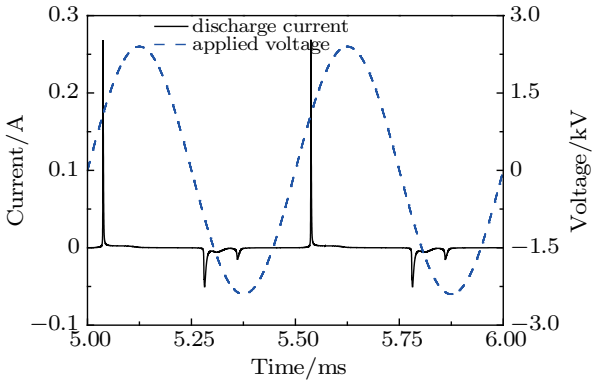


Fig. 4. (color online) Temporal dynamics of the voltage–current waveforms when the gas gap is reduced to 0.58 cm.

To better understand this asymmetry, we study the effect of the coaxial electrode structure on the discharge. For the purposes of this article, the extent of electrode structure asymmetry is defined as R_2/R_0. According to $R_2/R_0 = 1 + (d + d_B)/R_0$, the value of R_2/R_0 changes as R_0 changes when the gas gap d and dielectric layer thickness d_B are fixed, where d and d_B are the same as those of the discharge in Fig. 2. Figure 5 illustrates the variation of A_1/A_2 with R_2/R_0. We see in the figure that A_1/A_2 is almost directly proportional to R_2/R_0. As R_2/R_0 decreases from 4.0 to 1.01, the A_1/A_2 decreases from 4.54 to 1.003. The slope of this line is about 1.183. This implies that in atmospheric-pressure coaxial electrode single pulse DBD the current asymmetry depends on the asymmetric extent of electrode structure, namely, the ratio of the outer electrode radius to the inner electrode radius. When this ratio is close to unity, a symmetrical discharge can be obtained.

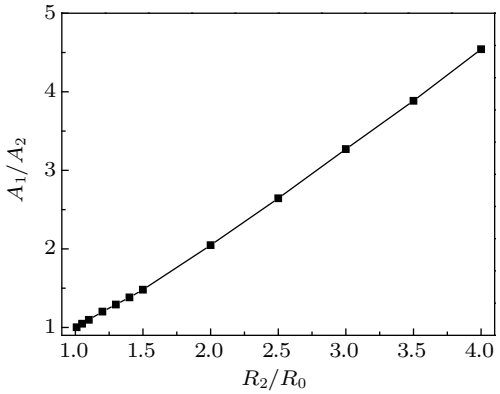


Fig. 5. Variation of A_1/A_2 with R_2/R_0.

More detailed calculations show that coaxial electrode DBD can present complex temporal nonlinearity with the increase of the driven frequency, which is consistent with the previous experimental results.[26] Figure 6 shows the plots of the discharge current evolving with the time at different frequencies, as well as their corresponding phase space trajectories. As shown in Fig. 6(a), the discharge turns into period-2 discharge through a bifurcation when the frequency is increased to 5.8 kHz. In the period-2 discharge, the repetition period of current doubles that of the applied voltage. This can be confirmed by two different loops in the phase space in Fig. 6(a). For the convenience of description, nP is used to represent the period-n state, in which the repetition period of current equals n cycles of the applied voltage. The 2P sustains a small frequency interval of about 2.5 kHz, and then bifurcates again into 4P at 8.3 kHz, see Fig. 6(b). In the 4P, one complete current oscillation period includes eight different current pulses, corresponding to four different loops in the phase space. After the discharge is replaced by 4P, the discharge becomes more unstable. The 4P only lasts 0.22 kHz before bifurcating into 8P, much shorter than 2.5 kHz of 2P. With frequency increasing further, the 8P sustains a very short

frequency interval, about 0.08 kHz, and then turns into chaotic state at 8.6 kHz, which is shown in Figs. 6(c) and 6(d). Once the discharge enters into chaos, the discharge current evolving with the time does not have obvious periodicity any longer. It fluctuates stochastically and the corresponding phase space trajectories in Fig. 6(d) become indistinguishable.

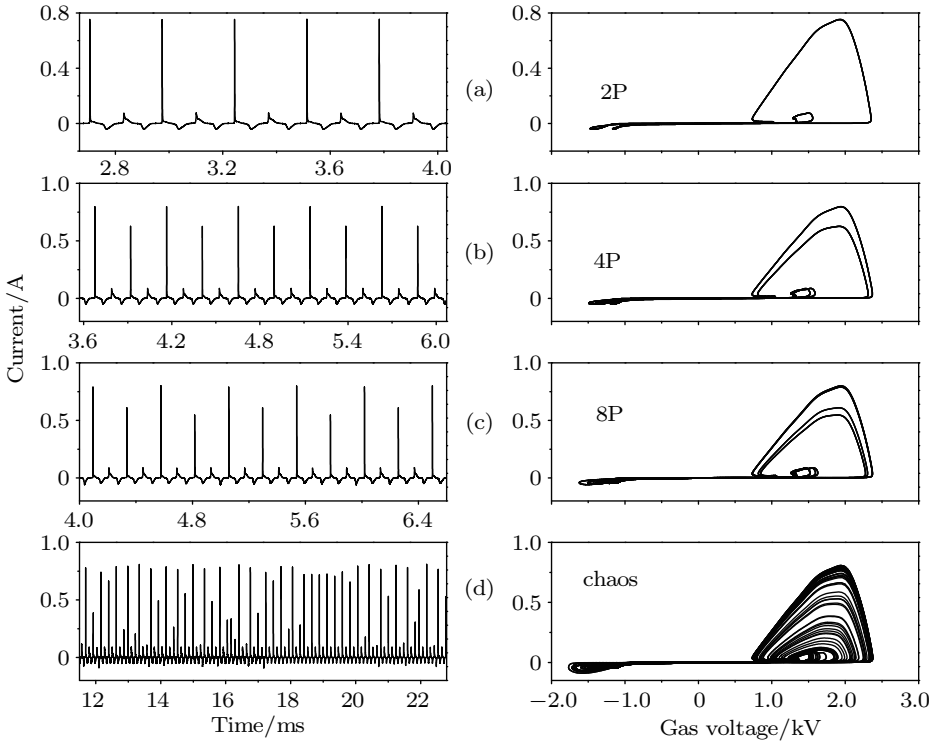


Fig. 6. Plots of the discharge current evolving with the time at different frequencies, and their corresponding phase space trajectories. Panels (a), (b), (c), and (d) correspond to 5.8 kHz, 8.3 kHz, 8.52 kHz, and 8.6 kHz, respectively.

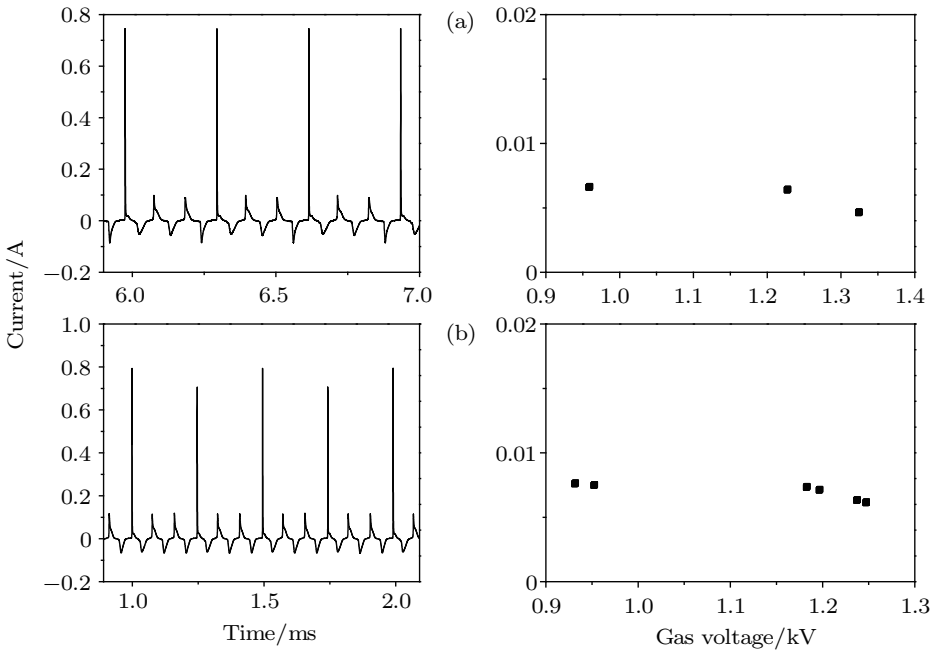


Fig. 7. Plots of the discharge current evolving with time at (a) 9.5 kHz, and (b) 11 kHz and their own Poincare sections.

The above results suggest that in the period-doubling bifurcation sequence the period-n discharge becomes more and more unstable with the increase of n. This conclusion can also be confirmed in other period-doubling bifurcation with the increase of the frequency. As the frequency is increased to 9.5 kHz, the chaotic state changes into 3P suddenly. The left diagram in Fig. 7(a) shows the plot of the discharge current evolving with time for this 3P. Obviously, the discharge current cycle is three times the voltage cycle. To identify exactly the periodic characteristic of discharge, the corresponding Poincare section is plotted in the right diagram in Fig. 7(a). Three scattered points clearly show that the discharge is a

period-3 discharge. According to the theory of Li–York, the 3P means the existence of chaos in the discharge system. Therefore, it indirectly proves that the route to chaos through period multiplication in Fig. 6 does exist. The 3P lasts from 9.5 kHz to 11.0 kHz, and finally changes into 6P at 11 kHz. In the 6P discharge, there are six discrete points on the Poincare section, see the right diagram in Fig. 7(b). This 6P discharge only sustains about 0.6 kHz and then transits into chaos again with the frequency increasing over 11.6 kHz. Clearly, in the secondary bifurcation 3P–6P the 3P is more stable than 6P, which is in good agreement with the above results.

In addition to the way of increasing the frequency, the period multiplication behaviors can also be observed by changing the gas width. Figure 8 shows the plots of the discharge current evolving with time at different gap widths, and their corresponding three-dimensional current–voltage–charge phase space trajectories. Here, the frequency is 5.0 kHz and the voltage is 2.4 kV. As shown in Fig. 8(a), the discharge is an asymmetric 1P discharge when the gas width is 0.6 cm, just like the discharge in Fig. 2. In the three-dimensional phase space, its trajectory is a closed curve with one convolution. As the gas width is increased to 0.8 from 0.6 cm, the discharge dynamic behaviors undergo an abrupt change (from Figs. 8(a) to 8(b)) in its three-dimensional phase space. This means that a bifurcation happens here. As the gas width is increased further to 1.0 cm, another bifurcation happens and the 2P is replaced by 4P. The number of convolutions in three-dimensional phase space becomes four, see Fig. 8(c).

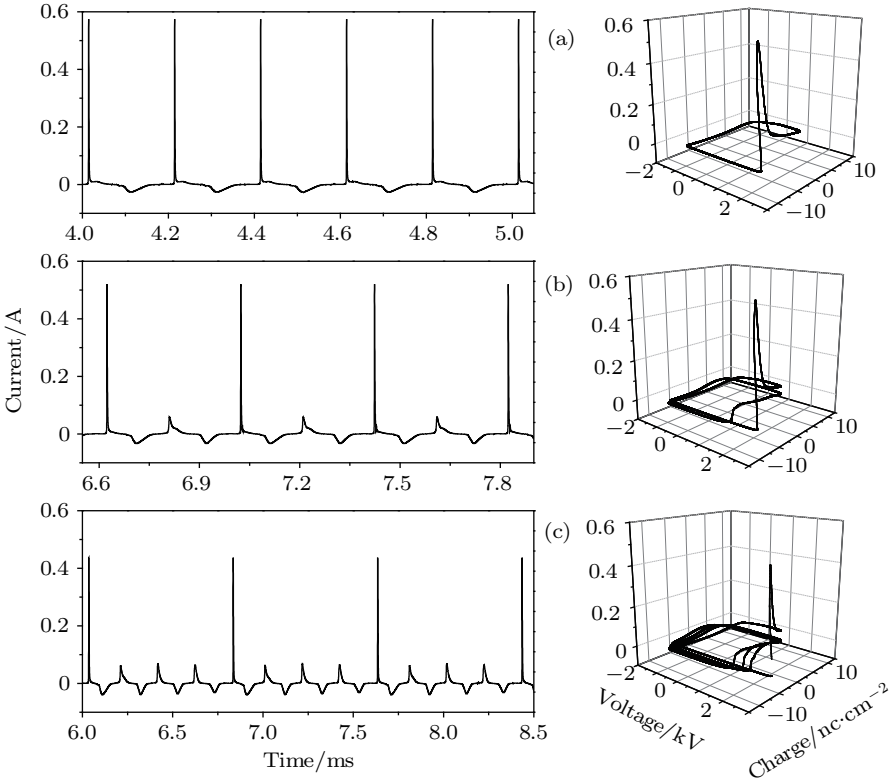


Fig. 8. Plots of the discharge current evolving with the time at different gap widths, and their corresponding trajectories in three-dimensional current–voltage–charge phase space. Panels (a), (b), and (c) correspond to 0.6 cm, 0.8 cm, and 1.0 cm, respectively.

It is known that the bifurcation of discharge current can be obtained by varying the exciting frequency or gas gap. But what are their underpinning physics mechanisms? Considering the complexity of this question, we take the bifurcation from 1P to 2P for example. To focus on how the bifurcation occurs, we further take a whole voltage period as an investigative unit. Figure 9 shows the spatial structures of the electron density, ion density, and electric field at some key times during this evolution. Figures 9(a) and 9(d) correspond to the times at the end of the first voltage period in Figs. 2 and 6(a), namely the applied voltage is close to zero from the negative value. Figures 9(b), 9(c), 9(e), and 9(f) correspond to the breakdown and peak current times of their own subsequent discharges. From Figs. 9(a)–9(c), we can see that the discharge develops first into a Townsend discharge and then transforms into glow discharge, and the discharge occurs in the whole gas gap. This correlates well with the numerical and experimental results.[20,25,27] So, the subsequent discharge current is large, see the third discharge current in Fig. 2. When the frequency is increased to 5.8 kHz, it is found that in Fig. 9(d) the spatial structures of the electron density, ion density, and electric field are very different from those in Fig. 9(a). A plasma positive column with high particle density accompanied by a distorted electric field appears in the discharge gap. This change can be

explained as follows. Increasing the frequency will lead to a stronger discharge, which will raise the charged particles density in the plasma positive column and electric field in the gas gap. On the other hand, less time interval between voltage periods at high frequency reduces the disappearance time of column and electric field. When the frequency is increased to a certain value, the column and electric field do not have enough time to vanish, as such this distribution can be formed. Once this distribution occurs, the subsequent discharge will have a fundamental change. The plasma column will act as an instantaneous anode, and shorten the discharge region. As shown in Figs. 9(d)–9(f), the discharge occurs mainly in 0.44 cm–0.8 cm. In this narrow region the discharge is a Townsend-like discharge, namely, the maximum electron density is located at the momentary anode and is much smaller than the ion density. As a result, the subsequent discharge current is very small, see the third discharge current in Fig. 6(a). This is consistent with the results of Ref. [25]. When the subsequent voltage period is over, the distributions of charged particles density and electric field return to the similar distributions in Fig. 9(a) again, as such the 2P in Fig. 6(a) is formed.

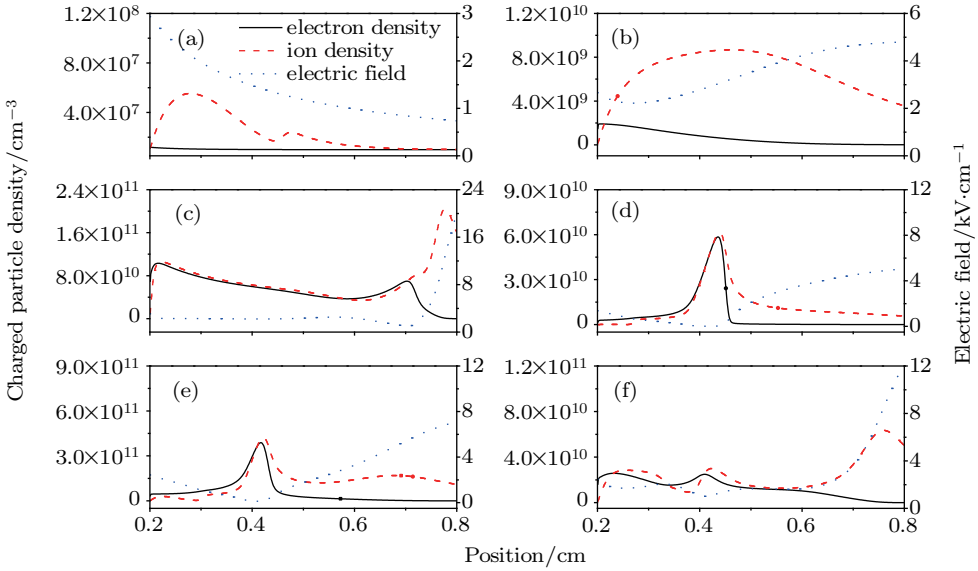


Fig. 9. (color online) Plots of spatial distributions of the electron density, ion density, and electric field at some key times: (a) at the end of the first voltage period in Fig. 2; (b) at the breakdown of the third discharge in Fig. 2; (c) at the occurrence of current peak of third discharge current in Fig. 2; (d) at the end of the first voltage period in Fig. 6(a); (e) at the breakdown of the third discharge in Fig. 6(a); (f) at the occurrence of current peak of third discharge current in Fig. 6(a).

Figure 10(a) shows the spatial structures of the electron and ion densities as well as the electric field at the end of the first voltage period in Fig. 8(b). It is clear that the plasma column has not completely vanished and the electric field is distorted. This is very similar to the distributions in Fig. 9(d). Thus the subsequent discharge current is weak, see the third discharge current in Fig. 8(b). The formation of the distribution in Fig. 10(a) can be attributed to the wider plasma column in the discharge with larger gas gap.[23] When the subsequent voltage period is over, the corresponding distributions of the electron density, ion density and electric field return to the similar distributions in Fig. 9(a). As shown in Fig. 10(b), there is no plasma positive column in the discharge gap, the electron density and ion density are both very low, and the electric field has no obvious distortion. As expected, the subsequent discharge current is large, see the fifth discharge current in Fig. 8(b). The spatial distributions in Figs. 10(a) and 10(b) appear alternately during the two voltage periods, which results in the formation of the 2P.

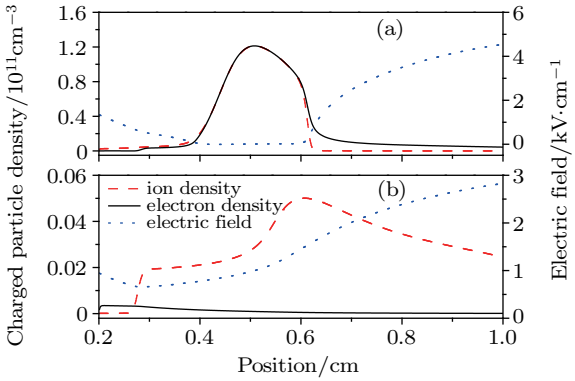


Fig. 10. (color online) Spatial distributions of electron density, ion density, and electric field at two key times in Fig. 8(b): (a) at the end of the first voltage period; (b) at the end of the second voltage period.

From the above discussion, it can be concluded that the residual quasineutral plasma from the previous discharges and corresponding electric field distribution can severely weaken the subsequent discharge. When the quasineutral plasma and electric field distribution appear at the end of one voltage period, it makes the 1P bifurcate into 2P. Similarly, when it appears at the end of two voltage periods, the 2P will bifurcate

into 4P. In other words, its appearance can result in the occurrence of bifurcation.

4. Conclusions

We study the characteristics and nonlinear behaviors of atmospheric-pressure coaxial electrode dielectric barrier discharges by using a one-dimensional fluid model. It is shown that the discharge is often asymmetrical between the positive current pulse and negative current pulse. When the outer electrode is the moment cathode, the corresponding discharge current is larger. The gas gap has an important effect on this asymmetry. The degree of this asymmetry decreases exponentially by reducing the gas gap. But it may not obtain a symmetrical single pulse discharge, because at small gas gap the multi-pulse discharge appears. This asymmetry is proportional to the extent of electrode structure asymmetry, namely, the ratio of the outer electrode radius to the inner electrode radius. When the ratio is close to unity, a symmetrical discharge can be obtained.

Improving the driven frequency, many nonlinear behaviors such as period-doubling bifurcation, chaos and secondary bifurcation can be obtained. The corresponding trajectory in phase space and Poincare sections are used to identify exactly the periodic characteristic of discharge. In the period-doubling bifurcation sequence the period-n discharge becomes more and more unstable with the increase of n. In addition, the period multiplication phenomenon can also be observed by changing the gas width. The underpinning mechanisms of these bifurcations are studied by the evolutions of the space charged particles and electric field. It is found that the residual quasineutral plasma from the previous discharges and corresponding electric field distribution can severely weaken the subsequent discharge, and leads to a bifurcation.

References

[1] Sira M, Trunec D and St'ahel P 2008 *J. Phys. D: Appl. Phys.* **41** 015205
[2] Fanelli F and Fracassi F 2016 *Plasma Process. Polym.* **13** 470
[3] Laroussi M 2002 *IEE Trans. Plasma Sci.* **30** 1409
[4] Penetrante B M, Bardsley J N and Hsiao M C 1997 *Jpn. J. Appl. Phys.* **36** 5007
[5] Kogelschatz U 2002 *IEE Trans. Plasma Sci.* **30** 1400
[6] Li X C, Zhang Q, Jia P Y, Chu J D, Zhang P P and Dong L F 2017 *Phys. Plasmas* **24** 033505
[7] Walsh J L, Iza F, Janson N B, Law V J and Kong M G 2010 *J. Phys. D: Appl. Phys.* **43** 075201
[8] Walsh J L, Iza F, Janson N B and Kong M G 2012 *Plasma Sources Sci. Technol.* **21** 034008
[9] Zhang J, Wang Y H and Wang D Z 2013 *Phys. Plasmas* **20** 082315
[10] Wang X Q, Dai D, Hao Y P and Li L C 2012 *Acta Phys. Sin.* **61** 230504 (in Chinese)
[11] Zhang D Z, Wang Y H and Wang D Z 2013 *Phys. Plasmas* **20** 063504
[12] Ward A L 1962 *J. Appl. Phys.* **33** 2789
[13] Deloche R, Monchicourt P, Cheret M and Lambert F 1976 *Phys. Rev. A* **13** 1140
[14] Kulikovsky A A 1994 *J. Phys. D: Appl. Phys.* **27** 2556
[15] Zhang D Z, Wang Y H, Sun J Z and Wang D Z 2012 *Phys. Plasmas* **19** 043503
[16] Zhang Y T and He J 2013 *Phys. Plasmas* **20** 013502
[17] Li X C, Niu D Y, Yin Z Q, Fang T Z and Wang L 2012 *Phys. Plasmas* **19** 083505
[18] Yin Z Q, Wang Y, Zhang P P, Zhang Q and Li X C 2016 *Chin. Phys. B* **25** 125203
[19] Scharfetter D L and Gummel H K 1969 *IEEE Trans. Electron Dev.* **16** 64
[20] Li X C, Niu D Y, Xu L F and Chang Y Y 2012 *Chin. Phys. B* **21** 075204
[21] Li X C, Zhao N, Fang T Z Liu Z H, Li L C and Dong L F 2008 *Plasma Sources Sci. Technol.* **17** 015507
[22] Zhang H Y, Wang D Z and Wang X G 2007 *Chin. Phys.* **16** 1089
[23] Dai D, Hou H X and Hao Y P 2011 *Appl. Phys. Lett.* **98** 131503
[24] Dai D, Wang Q M and Hao Y P 2013 *Acta Phys. Sin.* **62** 135204 (in Chinese)
[25] Ha Y, Wang H J and Wang X F 2012 *Phys. Plasmas* **19** 012308
[26] Qi B, Huang J J, Zhang Z H and Wang D Z 2008 *Chin. Phys. Lett.* **25** 3323
[27] Luo H Y, Liang Z, Lv B, Wang X X, Guan Z C and Wang L M 2007 *Appl. Phys. Lett.* **91** 221504